305

J. Electroanal. Chem., 153 (1983) 223–242
Elsevier Sequoia S.A., Lausanne – Printed in The Netherlands

POLYMER FILMS ON ELECTRODES

PART XII. CHRONOAMPEROMETRIC AND ROTATING DISK ELECTRODE DETERMINATION OF THE MECHANISM OF MASS TRANSPORT THROUGH POLY(VINYL FERROCENE) FILMS

JOHNA LEDDY and ALLEN J. BARD

Department of Chemistry, The University of Texas at Austin, Austin, TX 78712 (U.S.A.)

(Received 22nd November 1982; in revised form 31st January 1983)

ABSTRACT

Chronoamperometry was used to discriminate between two models describing mass transport of a solution species to an electrode surface through an electroinactive polymer layer. At potentials where poly(vinyl ferrocene) is not electroactive, a platinum disk modified with this polymer was used to examine the first reduction of methyl viologen dication (MV^{2+}) and of benzoquinone (BQ) in acetonitrile. The membrane model, as opposed to the pinhole model, was shown to be consistent with the chronoamperometric data; XPS and SEM results support this conclusion. Rotating disk electrode measurements were also consistent with the membrane model. A method to determine the thickness of the solvent-swollen polymer is discussed, and estimates of the redox couples' diffusion coefficients and extraction coefficients into the polymer based on this thickness were: $D_m(MV^{2+}) = 4 \times 10^{-8}$ cm^2/s; $D_m(BQ) = 1 \times 10^{-7}$ cm^2/s; $K(MV^{2+}) = 6$; and $K(BQ) = 4$.

INTRODUCTION

Reductions and oxidations of solution species at a polymer modified electrode in potential ranges where the polymer is not electroactive, have been treated theoretically by two distinct models. Both begin by treating the polymer as a finite layer interfaced with a semi-infinite region, the solution. The redox couple is present in the solution in both cases. Gueshi, Takuda and Matsuda [1] considered the case of channel diffusion for chronopotentiometry, chronoamperometry, and cyclic voltammetry. In this "pinhole model," the polymer is presented as an impervious layer on the electrode surface which contains many small pinholes. Mass transport of solution species to the electrode occurs by diffusion in the solution-filled channels. For the case of infinitesimally small channels, the polymer can be considered as a uniform phase (membrane) through which the solution species diffuses. One must also account for the extraction equilibrium of solution species between the polymer and solution. This membrane model, based on the assumption of rapid attainment of extraction equilibrium at the polymer/solution interface has been developed for

0022-0728/83/$03.00

chronoamperometry by Peerce and Bard [2a] and for steady state currents at a rotating disk electrode by Gough and Leypoldt [3a–c].

A previous study of poly(vinyl ferrocene) [2a] coated electrodes attempted to determine the mode of transport of a solution species through the film. Electron transfer through the polymer and mediated redox reactions were shown to be unlikely; a model based on membrane transport of solution species to the substrate was proposed. It then remained to differentiate between the membrane and pinhole models. The chronoamperometric data appeared to conform more closely to the membrane model. However, because of the very thin films considered in the study and a lack of information on the solvent swollen polymer, determination of polymer film parameters (e.g. diffusion or extraction coefficients) was not attempted. This paper discusses an examination of thicker films, both by chronoamperometric and rotating disk electrode (RDE) methods. These data also support the membrane model. Information on the swelling of the polymer was obtained by determining the weight of the minimum amount of solvent needed to wet the film. This information, in conjunction with the electrochemical results, allowed the extraction constant and diffusion coefficient of the solution species in the membrane to be determined.

EXPERIMENTAL

Materials

Acetonitrile and dichloromethane (both Matheson, Coleman and Bell, MCB) were dried over 0.4 nm molecular sieves. The electrolyte, tetrabutylammonium tetrafluoroborate, $TBABF_4$ (Southwestern Analytical Chemicals), was recrystallized from ethyl acetate, washed with ether, and dried under vacuum overnight. Methyl viologen hexafluorophosphate, $MV^{2+}(PF_6^-)_2$, was precipitated from aqueous $MV^{2+}(Cl^-)_2$ (Sigma) with saturated NH_4PF_6; it was recrystallized from MeCN/ether, and dried. Benzoquinone, BQ, (MCB) was recrystallized from hot hexane and air dried. Poly(vinyl ferrocene), PVF (MW 15,700 g; degree of polymerization 74), was prepared by Thomas W. Smith [4].

Apparatus

Electrochemical measurements were performed with a Princeton Applied Research Model 173 potentiostat, Model 175 universal programmer, and Model 179 digital coulometer. Solution resistance was compensated using positive feedback. All transients were recorded and stored on a Norland 3001 digital oscilloscope. It was necessary to record the data at several sampling rates because an accurate digitization of the current over the whole time window of interest could not be obtained at a single rate. This difficulty arose because the rapid decay of the transient yielded a current several orders of magnitude larger at early times than at later times. As a result, if the amplifier was set to make an accurate record of the later time data, it overloaded and the early time information was lost. To circumvent the problem,

transients were recorded at several sampling rates with the amplifier set to the greatest sensitivity possible without overload. In this way, the current over the time window of interest was accurately accessed by using the early time data from several transients, each taken at a different sampling rate. For example, if the first 100 points of a digitized transient are accurate, and a set of transients are recorded at 10^{-5}, 10^{-3} and 10^{-1} s/point, then a record of good accuracy and sensitivity is obtained from 10 μs to 10 s. The solid lines in Figs. 2 and 3 are plots of experimental data taken from a set of transients recorded at several sampling rates; the data handling capabilities of the Norland scope were used to do a seven point smooth on these curves and to plot current ratios. The jagged segments in the plots result as the limit of the Norland's digitizing ability (10 bits) is approached for each sampling rate. All cyclic voltammograms and outputs of the Norland scope were recorded on Houston Instruments 2000 x–y recorder. Rotating disk electrode measurements were made with a Pine Instruments ASR-2 rotator. A Mettler microbalance (Model M5) was used in weighing experiments to determine wetted film thickness. Electrochemical measurements were performed in a single compartment cell. Electrolyte concentration for MeCN solutions was usually 0.5 *M*, but never less than 0.1 *M*. Dichloromethane solutions were maintained at 0.1 *M*. Working electrodes were platinum disks. The area of the RDE was 0.458 cm^2; the electrode used in chronoamperometric experiments had an area of 0.035 cm^2. A platinum gauze counter electrode and a silver wire quasireference electrode were utilized. The quasireference electrode potential was approximately 100 mV negative of SCE. SEM samples were prepared using glassy carbon electrodes as graphite does not interfere with the microscopy measurements.

Procedure

PVF was electroprecipitated [5] from dichloromethane solution by potentiostating the system at +0.7 V vs Ag; during deposition, the RDE was spun or, for the platinum disk, the solution was stirred. A cylindrical counter electrode was used to enhance symmetric current distribution. The film coated electrode was allowed to dry for at least 5 min before being placed in a $TBABF_4$/MeCN solution. The amount of PVF adsorbed was calculated by integrating the area under a negative sweep of the film, taken at 2 mV/s, a scan rate in the thin film behavior region. The PVF electrode was then moved to a $TBABF_4$/MeCN solution containing the redox couple of interest, MV^{2+} or BQ; the first reduction step ($MV^{2+} \rightarrow MV^{+\cdot}$; $BQ \rightarrow BQ^{-\cdot}$) was studied in each case. To ensure equilibration of the redox species between the polymer and solution, the potential applied to the working electrode was cycled through E^0 of the redox species for 5 min. Following each potential perturbation, it was necessary to allow 2 min before beginning the next measurement to ensure the polymer had relaxed back to its equilibrium state. Before beginning an experiment, solutions were purged with prepurified nitrogen passed over R3-11 catalyst (Chemalog); solutions were blanketed with nitrogen during the course of the experiment. Reduction of MV^{2+} is extremely sensitive to oxygen. All potential step measure-

ments at a stationary electrode were, therefore, carried out in a closed cell. As the cell for rotating disk experiments was necessarily open, these experiments were performed in a glove bag.

One set of SEM measurements were performed on copper electroprecipitated onto polymer modified glassy carbon electrodes. These samples were prepared by electrodepositing a 2 μm thick PVF film onto a glassy carbon electrode. The electrode was placed into a solution of MeCN saturated with cupric acetate (MCB) and containing sodium acetate (MCB), where the film was reduced to the ferrocene form. The electrode was then potentiostated at -0.7 V vs. SCE until 0.15 C had passed. After drying, the electrode was soaked in dichloromethane to remove the PVF film. Copper films deposited on glassy carbon in the absence of the polymer were also soaked in dichloromethane.

RESULT AND DISCUSSION

The following is a review of the major theoretical points of the pinhole and membrane models for chronoamperometry. An evaluation of the experimental results shows the data to be consistent with the membrane model. Based on this model, the characteristic equation and experimental results for steady state RDE measurements are presented. Scanning electron microscopy (SEM) and X-ray photoelectron spectroscopy (XPS) support the conclusion that mass transport occurs by diffusion in the membrane. A method to estimate the degree of swelling and thickness of the solvent-soaked polymer is also discussed.

CHRONOAMPEROMETRY

Pinhole model

The salient characteristics of the pinhole model for chronoamperometry have been outlined previously [1,2a]. Briefly, for a surface coverage, θ, greater than 0.5, the current at the polymer modified electrode, $i(\tau)$, normalized by the current at the bare electrode, $i_d(\tau)$, is

$$\frac{i(\tau)}{i_d(\tau)} = \left[\frac{1}{\sigma^2 - 1}\right]\left\{\sigma \exp(-\tau) - 1 + \sigma^2\left[\frac{\pi\tau}{\sigma^2 - 1}\right]^{1/2} \exp\left(\frac{\tau}{\sigma^2 - 1}\right)\left[\operatorname{erf}\left(\frac{\sigma\tau^{1/2}}{(\sigma^2 - 1)^{1/2}}\right) - \operatorname{erf}\left(\frac{\tau^{1/2}}{(\sigma^2 - 1)^{1/2}}\right)\right]\right\} \quad (1)$$

where $\sigma = \theta/(1 - \theta)$, $\tau = lt$, and l, as defined in ref. 1a, is dependent on the diffusion coefficient in the solution, D_s, the radius of the pinholes, a, a parameter g, and the coverage; $l = 2D_s/a^2\,\theta \ln(1 + g/(1 - \theta)^{1/2})$. θ and l are the parameters of interest. It

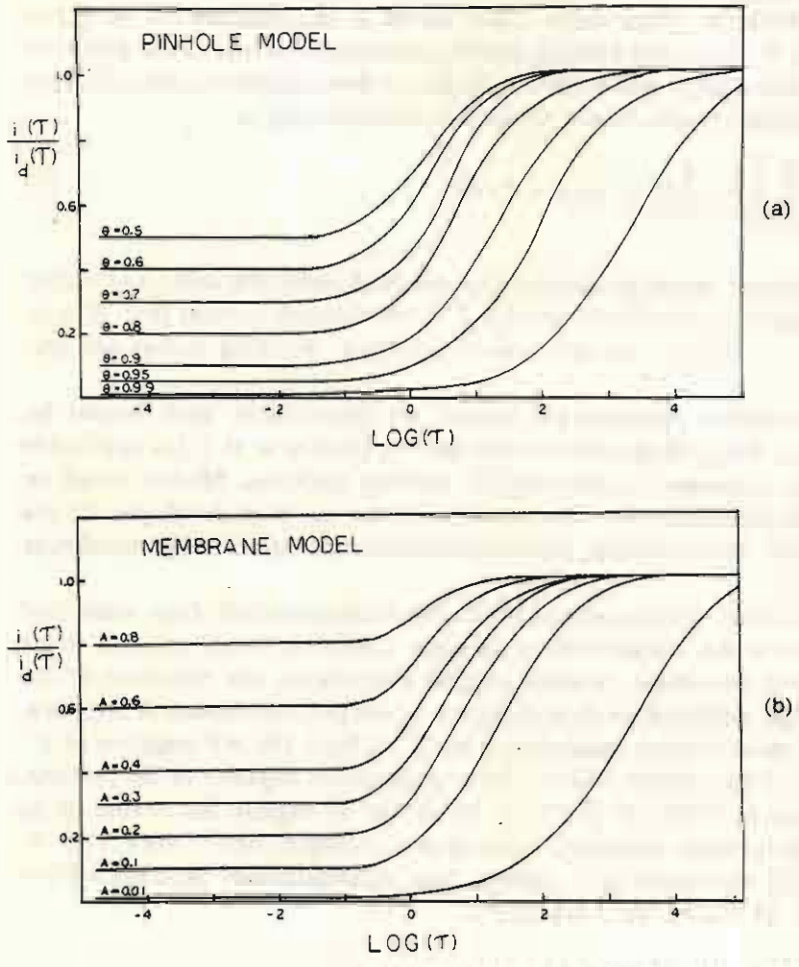

Fig. 1. Working curves for (a) the pinhole model and (b) the membrane model: $i(\tau)$ is the current passed at the polymer modified electrode and $i_d(\tau)$ is that at the bare electrode. θ is the surface coverage and A equals K/γ. τ is the dimensionless time for each model, lt for pinhole and $D_m t/\delta^2$ for membrane.

has been shown [2a] that for high coverage (greater than 90%), holes 1 nm in diameter are the limit accessible by practical chronoamperometric measurements. Working curves for $\theta > 0.5$ are shown in Fig. 1a.

Membrane model

The membrane model is based on a two-phase system, polymer and solution, where mass transfer occurs by diffusion in both phases. Material transport across the polymer–solution interface is assumed to be fast relative to diffusion, so that $c_m(\delta, t) = Kc_s(\delta, t)$ holds at all times; K is an extraction coefficient, δ is the

thickness of the wetted polymer, and $c_m(x, t)$ and $c_s(x, t)$ are the concentration in the polymer and solution, respectively. Each phase is also assigned a diffusion coefficient, D_m and D_s. As in the pinhole model, potential steps are to the diffusion limited plateau of the solution redox couple. Based on these conditions, the theoretical equation for current transients at a stationary electrode [2a] is:

$$\frac{i(\tau)}{i_d(\tau)} = \frac{K}{\gamma}\left[1 + 2\sum_{j=1}^{\infty}\left[\frac{1 - K/\gamma}{1 + K/\gamma}\right]^j \exp(-j^2/\tau)\right] \quad (2)$$

where $i(\tau)$ is the current passed at the polymer modified electrode, and $i_d(\tau)$ is that at the bare electrode; $i_d(t) = nFAD_s^{1/2}c_s^*[\pi t]^{-1/2}$, the Cottrell current [6a]. $K/\gamma = K[D_m/D_s]^{1/2}$ and $\tau = D_m t/\delta^2$ are the values of interest. Working curves are presented in Fig. 1b.

A number of different pinhole-type models are conceivable, each bound by different constraints. The pinhole model developed by Gueshi et al. [1] is applicable for pinholes having a diameter on the order of the film thickness. Models based on increasingly smaller pinholes can be envisioned but have not been developed. In the case of infinitesimally small pinholes, the pinhole concept collapses to the membrane model.

The two models above, in conjunction with chronoamperometric data, were used to determine how a redox species moves through a polymer from solution to be reduced at the electrode surface. A third possible mechanism, the reduction of the redox couple through mediated electron transport at the polymer–solution interface, was eliminated by using solution species with an $E°$ at least 180 mV negative of $E°$ for the polymer [7]. Only couples with a reduction potential negative of the polymer were examined because PVF ($E° = 0.54$ V vs. SSCE) is slightly less stable in its oxidized form. The couples examined were methyl viologen, $MV^{2+}/MV^{+\cdot}$, $E° = -0.42$ V vs. SSCE, $D_s = 8.6 \times 10^{-6}$ cm^2/s) and benzoquinone. $BQ/BQ^{-\cdot}$ ($E° = -0.45$ V vs. SSCE, $D_s = 1.9 \times 10^{-5}$ cm^2/s).

EXPERIMENTAL RESULTS

Analysis of the chronoamperometric data for each model was carried out by normalizing the experimental current at the polymer modified electrode, $i(t)$, to that at the bare electrode $i_d(t)$, and plotting this ratio vs. $\log(t)$. The theoretical curves for the two models have very similar shapes (see Fig. 1); once the theoretical curves for both models have been fitted to the experimental results, the major distinction arises in the constant ratio $i(\tau)/i_d(\tau)$ as τ approaches zero (i.e., at short times). Unfortunately, these experimental ratios are inaccessible as they occur at times where double layer charging makes an appreciable contribution to the measured currents and potentiostat-cell rise times must be considered. We determined when the system is under diffusion control and the appropriate time range for measurements by finding the region where the Cottrell equation (eqn. 3) was obeyed at a

bare electrode.

$$it^{1/2} = nFAc_s^* D_s^{1/2} \pi^{-1/2} \quad (3)$$

In this region, a plot of $i_d(t)t^{1/2}$ vs. $\log(t)$, should yield a line of zero slope; positive deviations occur at short times due to double layer charging and at long times due to natural convection and edge diffusion. Results for 2 mM BQ are given in Fig. 2a, where dashed lines mark the region of zero slope (deviation $< \pm 2\%$). The times within this region of zero slope were used to examine the plot of $i(t)/i_d(t)$ vs. $\log(t)$ (see Fig. 2b). If $i_d(t)t^{1/2}$ is allowed to deviate more than $\pm 2\%$, fitting $i(t)/i_d(t)$ to the model curves becomes inexact. In fitting the experimental data to the theoretical working curves, the difference between $\log(\tau)$ and $\log(t)$ yields, for the pinhole model, $\log(l)$ and for the membrane model, $\log(D_m/\delta^2)$. Further, the ratio of $i(t)/i_d(t)|_{t\to 0}$ inferred by the curve fitting is equal to $(1-\theta)$ for the pinhole and K/γ for the membrane model.

Figures 2b and 3 show the fit of the theoretical curve for each model to representative chronoamperometric data. In fitting the data, theoretical curves with K/γ or θ equal to an integer multiple of 0.1 were used. The best fit was based on the rising portion of the theoretical curve which most closely matched the gradient of the experimental data. The parameters extracted for a set of film thicknesses at different concentrations of the solution redox couples are shown in Table 1. The reported thickness, d, is the dry thickness, calculated from a density of 1.25 g/cm^3 [8] and the charge passed during a negative sweep of the film at 2 mV/s. Two additional parameters of the pinhole model, a, the pinhole radius, and, R, half the distance between adjacent pinhole centers, are also cited in Table 1. These are calculated from $a^2 = 2D_s/l\theta \ln[1 + g/(1-\theta)^{1/2}]$ and $R^2 = a^2/(1-\theta)$. The experimentally inaccessible parameter, $g = \epsilon/(1-\epsilon)$ for $0 < \epsilon < 1$, accounts for radial diffusion and is taken as 1. In general, for the pinhole model, $\theta = 0.9$, indicating any pinholes have radii on the order of microns. Data analysis based on the membrane model shows K/γ is 0.4 for MV^{+2} and 0.3 for BQ. Table 1 shows there is no systematic dependence of any extracted parameters on concentration of the solution redox couple; this is consistent with both models. Gueshi's pinhole model for pinholes on the order of the film thickness, (consistent with the values extracted here), encompasses no dependence on the film thickness for θ or l, while the membrane model necessitates D_m/δ^2 be proportional to d^{-2}, assuming the polymer swells linearly. Examination of the data for a given value of θ shows l is inversely proportional to thickness, while $D_m d^2/\delta^2$ is approximately constant for a given redox couple. Based on this result, and evidence outline below, the mechanism of mass transport is best represented as membrane diffusion.

Two comments regarding the data in Figs. 2b and 3 remain to be made. Some variations in the time window for diffusion control is observed in these plots. At short times, variations in the electrolyte concentration changes the decay rate of the charging current, determining when the system comes under diffusion control. Variable vibrations of the lab bench account for long time variations. As shown in Figs. 1b and 2b, the experimental $i(t)/i_d(t)$ as $t \to 0$ lies consistently below K/γ.

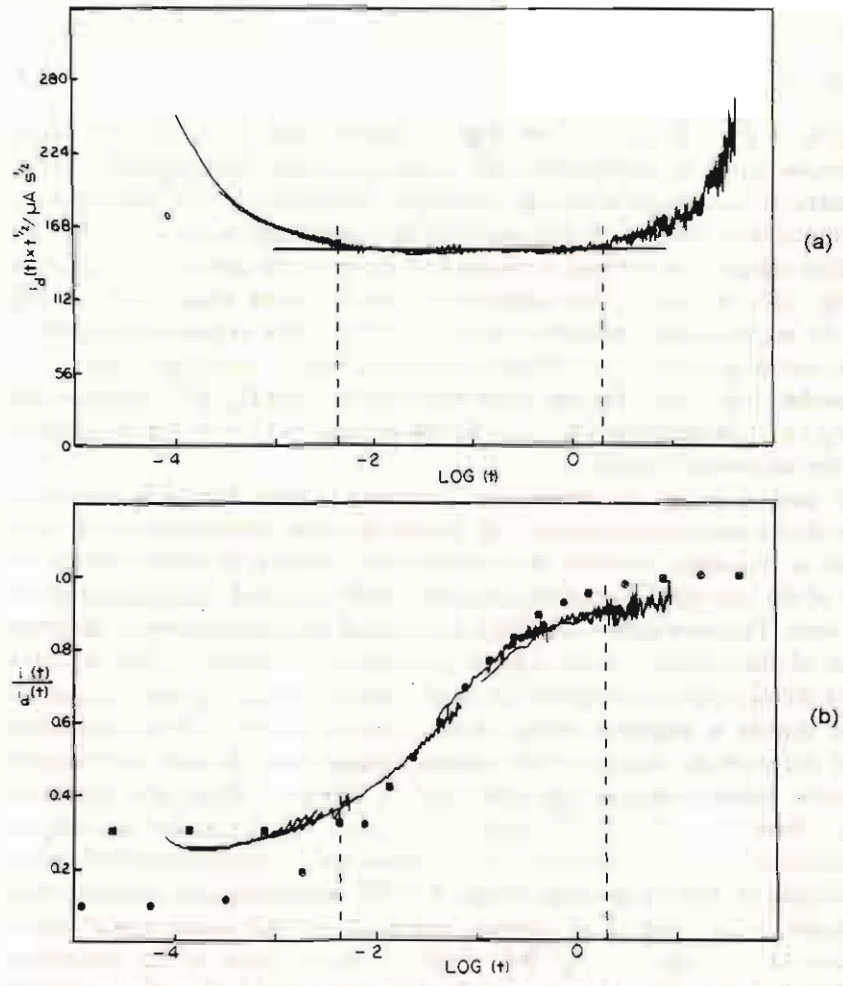

Fig. 2. Chronoamperometric data for the reduction of 1.92 mM benzoquinone in $TBABF_4$/MeCN. (a) A plot of $i_d(t)t^{1/2}$ vs. $\log t$, where $i_d(t)$ is the current passed at the bare electrode, exhibits a linear region when mass transfer obeys the Cottrell equation; the broken lines bound this time range. (b) A plot of $i(t)/i_d(t)$ vs. $\log t$, where $i(t)$ is the current passed at the PVF modified electrode. $d_{dry} = 2.33 \times 10^{-5}$ cm. Theoretical curves have been fitted using the data between the broken lines. The pinhole model (●) implies $\theta = 0.9$; the membrane model (■) implies $K/\gamma = 0.3$.

The resistance compensation used for these measurements was that of the bare electrode; frequently, this amount of compensation caused slight ringing in the transient of the polymer modified electrode at very short times, indicating the charging current decays faster in the polymer than in the solution. Thus, at short times, the polymer current is predominantly a faradaic current, while current at a bare electrode contains both faradaic and capacitive components, so that $i(t)/i_d(t)$ lies below the theoretical K/γ.

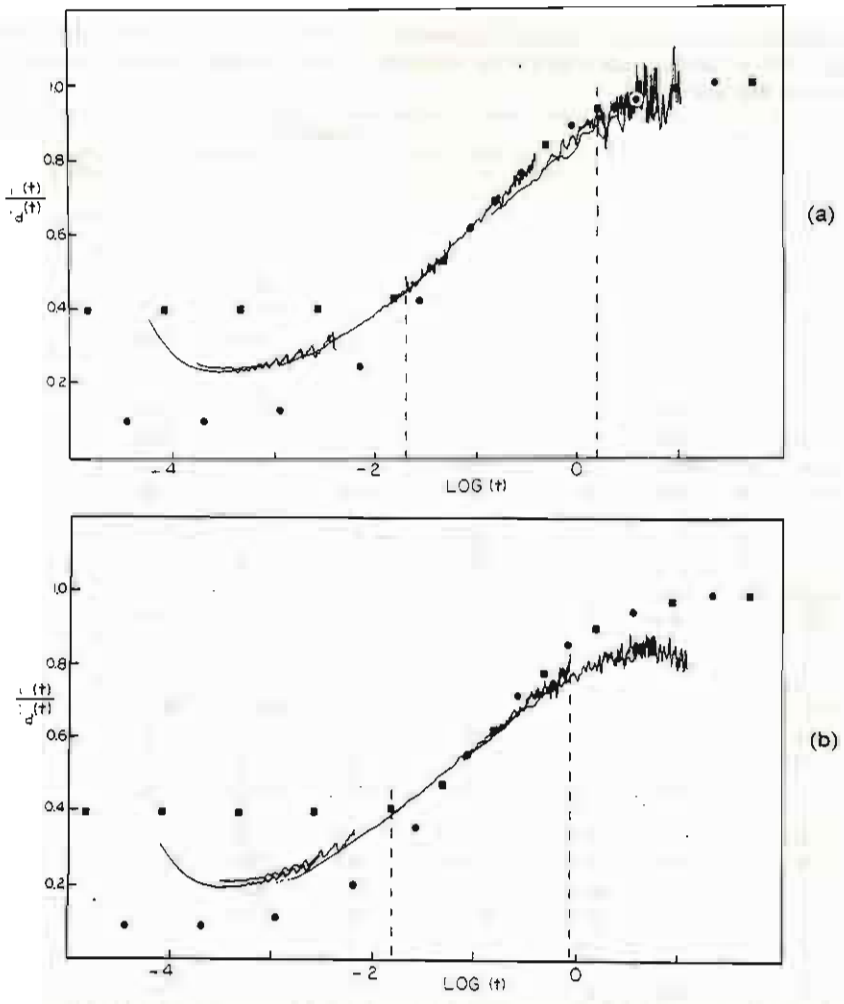

Fig. 3. Chronoamperometric data, $i(t)/i_d(t)$ vs. $\log t$, for the reduction of MV^{+2}. Theoretical curves were fit as in Fig. 2. The film has a dry thickness of 2.31×10^{-5} cm. c^* is (a) 1.76 mM; (b) 3.14 mM. The pinhole model (●) yields $\theta = 0.9$; the membrane (■) indicates $K/\gamma = 0.4$.

Charging current measurements at both bare and polymer coated electrodes (in the absence of electroactive species in solution) also show a lower resistance and capacitance for the coated electrode. Early time current transients (0 to 400 μs) taken in MeCN/TBABF$_4$ without resistance compensation have been analyzed based on a series RC circuit; $i = (E/R)\exp(-t/RC)$. The results indicate that with a polymer coating ($d \sim 1.27$ μm) the capacitance is 65% and the resistance is 70% of the bare electrode values. The pinhole model requires maintenance of the same

TABLE I

Analysis of chronoamperometric data for pinhole and membrane models. Most valves of a and R were calculated using $\theta = 0.9$; an asterisk indicating $\theta = 0.8$ was used. D_m was evaluated using $K/\gamma = 0.4$ for MV^{+2}, $K/\gamma = 0.3$ for BQ, and $\xi = 1.8$

		Pinhole				Membrane		
$10^5\, d_{dry}$/cm	c_s^*/ mM	θ	l	$10^5\, a$/cm $g = 1$	$10^3\, R$/cm $g = 1$	K/γ	D_m/δ^2	$10^8\, D_m$/cm^2 s^{-1}
MV								
2.31	0.77					0.4	66.8	11.5
	1.76	0.9	537.0	15.7	49.6	0.4	29.9	5.17
	2.40	0.9	269.2	22.1	69.8	0.4	16.4	2.84
	3.14	0.9	309.0	20.7	65.4	0.4	16.4	2.84
3.41	0.77	0.7	389.1	18.4	58.1	0.4	17.6	6.63
	1.76	0.8	309.0	20.7	65.4	0.3	6.8	2.56
	2.40	0.9	389.1	18.4	58.1	0.4	14.3	5.39
	3.14	0.8	239.9	23.5	74.3	0.4	11.9	4.48
6.49	2.18	0.8	48.9	51.9	164.0	0.3	1.7	2.39
	3.11	0.8	35.4	61.0	192.8	0.3	1.8	2.50
	4.35	0.9	40.7	56.9	179.8			
	4.95	0.9	23.4	75.0	237.0	0.4	1.2	1.65
BQ								
2.33	0.9					0.3	206.6	36.5
	1.92	0.9	851.1	18.5	58.5	0.3	90.2	15.9
	2.90	0.9	660.7	21.0	66.4	0.3	71.9	12.7
	3.97	0.9	398.1	27.0	85.3	0.3	42.3	7.45
3.92	1.94	0.8	38.0	88.2*	197.6*	0.3	29.4	14.6
	3.42	0.8	46.7	79.6*	178.3*	0.3	23.0	11.5
	5.01	0.8	63.1	68.5*	153.4*	0.3	32.2	16.0
	9.11	0.8	32.3	95.6*	214.1*	0.3	17.5	8.71
5.99	0.9						50.1	58.3
	1.92	0.9	346.7	28.9	91.3	0.4	38.7	45.0
	2.90	0.9	398.1	27.0	85.3	0.3	49.9	58.1
	3.97	0.9	269.2	32.8	103.6	0.3	30.7	35.8
7.70	5.82	0.8	16.2	135.0*	302.0*	0.3	7.5	14.5

charge density for both the bare and polymer modified electrodes; to account for the reduced capacitance, approximately 30% of the electrode surface would have to be blocked. This finding does not support the pinhole model, since 30% coverage is low compared to the $\theta = 0.9$ obtained from chronoamperometric measurements and this model. The reduced capacitance can be accounted for by the membrane model, if the polymer–metal and polymer–solution interfaces act as series capacitators or the double layer capacitance at the metal/polymer interface is decreased. The mem-

brane model of PVF modified electrodes has indicated that the diffusion coefficients, and, thus, the mobilities, of species extracted into the polymer are lower. However, the lower resistance found with the polymer suggests that the polymer is more conductive than the solution, despite the reduced mobility of the electrolyte. An enhancement of the electrolyte concentration would be necessary for the polymer to have higher conductance than the solution. This enhancement would be consistent with a polymer which extracts electrolyte as well as redox couple.

ROTATING DISK ELECTRODE MEASUREMENTS

RDE measurements can substantiate that transport through the film is best represented as diffusion in a membrane. Gough and Leypoldt [3] recognized for a polymer modified rotating disk that low rotation rates allow flux from the solution to establish a steady state current dependent on the square root of rotation rate, while high rotation rates confine the diffusion layer to the polymer, causing the steady state current to be independent of the rate of rotation. They derive [3a]:

$$\frac{1}{i_{lim}} = \frac{1}{0.62nFAc_s^* D_s^{2/3} \nu^{-1/6} \omega^{1/2}} + \frac{\delta}{nFAKc_s^* D_m} \tag{4}$$

where i_{lim} is the steady state limiting current passed at a rotating polymer modified electrode potentiostated on the plateau of the wave for reduction of the solution species 300 mV negative of E° for the solution species. The term $0.62nFAc_s^* D_s^{2/3} \nu^{-1/6} \omega^{1/2} = i_{lev}$ is the Levich current, which applies to current passed under the same conditions in the absence of the polymer. The permeability, $P_m = KD_m/\delta$, in the second term, is the parameter to be extracted. Similar measurements through ultrathin poly$\{Ru(bipy)_3\}^{2+}$ films have been made by Ikeda et al. [9]. Gough and Leypoldt [3d] also derived the characteristic equation for current transients at the RDE; however, the information obtained by this technique is the same as that found by chronoamperometry. A plot of i_{lim}^{-1} for a polymer modified electrode vs. $\omega^{-1/2}$ has the same slope as a similar plot for a bare electrode and a positive intercept dependent on the permeability of the film (Fig. 4). Such plots, for several film thicknesses, each at several concentrations, have been analyzed, and the resulting parameter, P_m, is shown in Table 2. The permeability decreases systematically with concentration, with effects being most significant at low concentration. Despite the error being systematic, all values for P_m for each thickness are well within an order of magnitude and represent no greater error than the random error found in the chronoamperometric measurements. $KD_m d/\delta$ is approximately constant for BQ; only one value was determined for MV^{2+}.

An analysis of rotating disk data based on the pinhole model can be made using the treatment of Landsberg et al. [10a–c]. They derive an expression for i_{lim} at an RDE where the fraction of the electrode surface active for electrolysis is confined to circular sites (pinholes).

$$\frac{1}{i_{lim}} = \frac{1.61\nu^{1/6}}{nFAD_s^{2/3} c_s^* \omega^{-1/2}} + \frac{\Sigma A_n \tanh\left[\frac{x_n \delta_o}{r_2}\right]}{nFAD_s c_s^*} \tag{5}$$

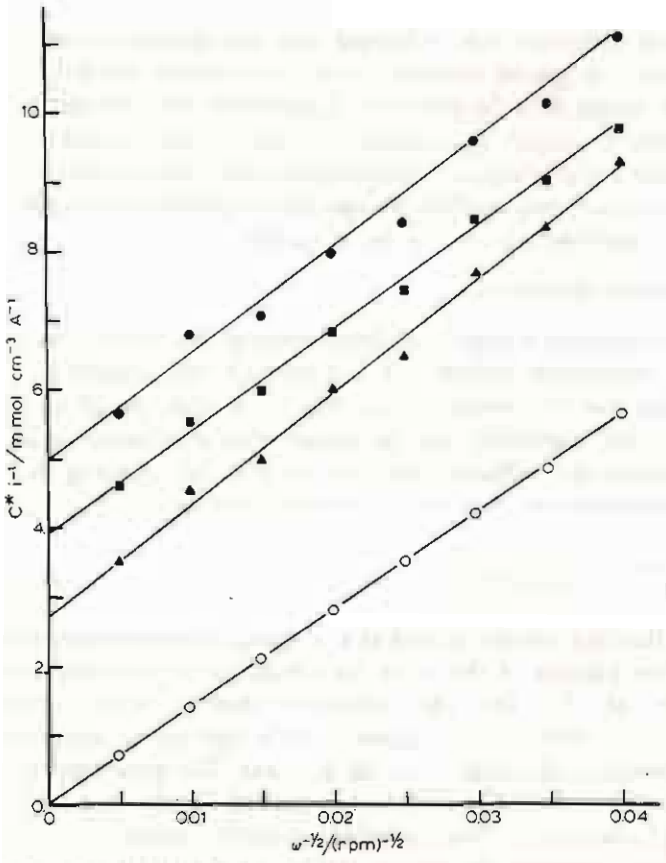

Fig. 4. Rotating disk data for the reduction of BQ. The reciprocal steady state current, normalized to the concentration, is plotted vs. $\omega^{-1/2}$. The polymer coated electrode, $d_{dry} = 7.70 \times 10^{-5}$ cm, was examined at (▲) 1.96 mM, (■) 3.84 mM, and (●) 5.82 mM; the bare Pt electrode was studied at (○) 5.82 mm. The intercept for the PVF modified electrode is proportional to P_m^{-1}.

where r_1 is the radius of an active site and $2r_2$ is the distance between centers of adjacent sites. $\delta_o = 1.61\ D_s^{1/3}\nu^{1/6}\omega^{-1/2}$, and is measured from the polymer–solution interface. A_n is a function of r_1, r_2 and x_n, where x_n represents the zero points of first-order Bessel functions. An analysis based on a plot of i_{lim}^{-1} vs. $\omega^{-1/2}$ has an intercept of $\Sigma A_n \tanh[x_n\delta_0/r_2]/(nFAc_s^*D_s)$. In the limiting case where $\delta_0 > r_2$, $A_n \tanh[x_n\delta_0/r_2] \rightarrow A_n$; when $\delta_0 < r_2$, $A_n \tanh[x_n\delta_0/r_2] \rightarrow A_n x_n\delta_0/r_2$, and, as δ_0 is linearly dependent on $\omega^{-1/2}$, a plot of i_{lim}^{-1} vs. $\omega^{-1/2}$ will have an intercept of zero and a slope of $1.61\ \nu^{1/6}(1 + A_n x_n/r_2)/nFAc_s^*D_s^{2/3}$. In the intermediate region, $\delta_0 \sim r_2$, i_{lim}^{-1} vs. $\omega^{-1/2}$ is nonlinear; given the approximate value of r_2 from δ_0, and the value of A_n, r_1 can be evaluated from a working curve [10a]. There are difficulties with Landsberg's model, however, because no account is taken of radial diffusion. This model is, therefore, accurate in two limiting cases; (i) many small (r_1, $r_2 < \delta_0$)

pinholes, and (ii) a few large acentrically placed pinholes ($r_1, r_2 > \delta_0$). A_n is such that in case (i), in lim $A_n(r_1 \rightarrow r_2)$ $A_n = 0$, and in case (ii) i_{lim} has a representation similar to a rotating ring electrode; for i_{lim}^{-1} vs. $\omega^{-1/2}$, both these situations ensure an intercept of zero.

Plots of experimental i_{lim}^{-1} vs. $\omega^{-1/2}$ for the polymer modified RDE shows a nonzero intercept and the same slope as a similar plot for a bare electrode. The nonzero intercept and slope indistinguishable from a bare electrode eliminate case (ii). The experimental points are linear over the total range of $\omega^{-1/2}$, indicating δ_0 is always greater than r_2 and, thus, $r_2 < 2 \times 10^{-4}$ cm. Normalizing the intercept according to Landsberg's model, ΣA_n is 6×10^{-3} cm. This indicates that if r_2 is of the order of μm, the pinholes are of the order to 10 nm; if r_2 is less than 1 μm, the sizes of the pinholes approaches zero. This illustrates the collapse of the pinhole model to the membrane case in the limit of very small pinholes, and, again, supports the membrane model.

OTHER SUPPORTIVE EVIDENCE

Other techniques have been applied to the poly(vinyl ferrocene)/MeCN system with a twofold intent. That is, first, to help substantiate mass transport in the film is predominantly by membrane diffusion and, second, to show, if possible, mass transport is solely by membrane diffusion. The first objective has been pursued by employing the spectroscopic techniques of XPS and SEM. Analysis of the chronoamperometric data based on the pinhole model showed any pinholes in the film have a radius on the order of 1 μm, while the dry film thickness is on the order of 0.1 μm. This indicates any channels in the polymer are not tortuous, and, in conjunction with the coverage, implies that the platinum substrate should be observable through the film. XPS, however, reveals no platinum, suggesting $\theta > 0.98$ [2a]. Scanning electron microscopy of the dry films finds evidence of channels up to 0.5 μm in diameter [2a]. The dry film characteristics, however, will not necessarily correlate with the properties of the wetted polymer.

A second SEM experiment has been performed, which better characterizes the wetted polymer. Consider electrodepositing a copper film at a PVF modified electrode. In a case of strict pinhole diffusion, SEM would be expected to show copper deposited in isolated islands, whereas a strict membrane diffusion should display a uniform coating of copper. The sensitivity of SEM requires a coating of copper which is at least 2.5×10^{-5} cm thick, and PVF is not well characterized for films more than approximately 2 μm thick. Within these constraints, a layer of copper approximately 0.25 μm thick, based on the total surface area of the glassy carbon electrode, was plated from a quiescent solution through a 2 μm thick PVF film; the PVF was then removed by soaking in dichloromethane. Copper was also deposited on glassy carbon. The results of this experiment are presented in the micrographs: Figure 5a, copper deposited on glassy carbon, and Fig. 5b, copper deposited through PVF on a similarly rough piece of glassy carbon. Stereoscopic imaging shows the dark circular regions to be concavities, resulting, perhaps, from

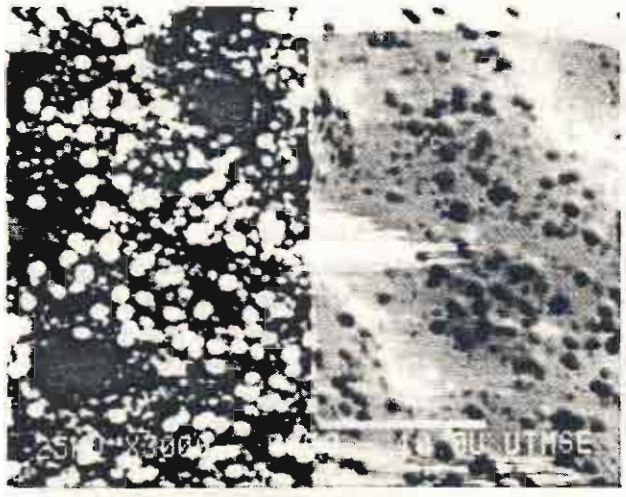

(a)

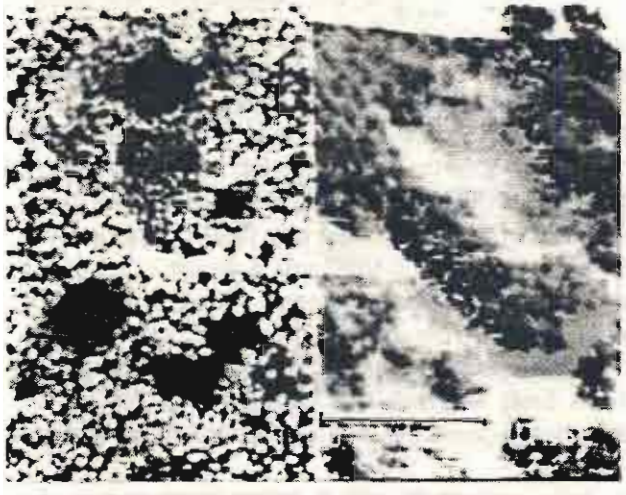

(b)

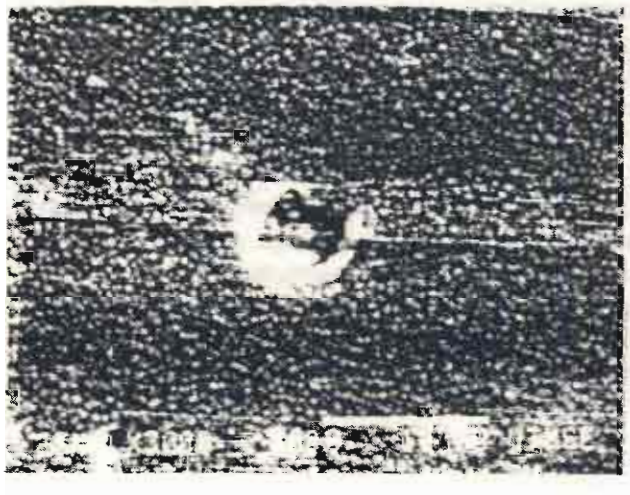

(c)

imperfections in the graphite substrate. Columnar depressions in the copper layer are inconsequential for both models. The copper deposited fairly uniformly over the surface, independent of the polymer's presence. The small beadlike structure of the deposit must result from the solvent, MeCN, as experiments in water gave a more uniform distribution of copper. X-ray dot mapping shows the copper is distributed with equal uniformity over the surface, with or without the polymer; it also shows little or no iron on the surface, indicating the PVF has been removed by the soaking in dichloromethane. Copper deposited through PVF onto a piece of glassy carbon cut from the highly polished end of a rod (Fig. 5c) produces a highly uniform coating, which also contains a concavity. Copper has deposited on the inside of this depression, as it did in the two previous cases. In each of these micrographs, imperfections in the surface had been sought out; in general, the surface had fewer imperfections than these micrographs indicate. As shown in Fig. 5, the polymer does not alter the nature of the copper deposition, the SEM results are consistent with the membrane model.

The second question remains, however, as to whether the deposition occurs solely by membrane diffusion or a combination of pinhole and membrane diffusion. Ideally, in the latter case, the micrograph would show a homogeneously covered background resulting from membrane control, and stalagmite structures protruding from the background, caused by deposition in the pinholes. However, under the conditions of the deposition, it is highly unlikely that the height of the stalagmite structure would be sufficiently distinct from the background for SEM to be useful in determining to what extent pinhole diffusion contributes to the deposition process. Examination of Fig. 5c shows a very uniform coating of copper, indicating diffusion in the membrane is the predominant mode of mass transfer, but minor contributions from pinhole diffusion cannot be ruled out.

Several other approaches have been considered in an attempt to show that mass transport is solely by membrane diffusion. Generally, these have substantiated that the wetted polymer behaves as a viscous liquid, but have not precluded the presence of pinholes. The existence of pinholes could be rejected if a solution moiety could be found which does not extract into the polymer. However, PVF is sufficiently well wetted by the MeCN that its character is not drastically distinct from the solvent and, as a result, K has been found to be non-zero with many other substrates (e.g., nitrobenzene, thianthrene, transition metal chelates). Low dielectric solvents, such as tetrahydrofuran, were not helpful. Alternatively, a second electroactive polymer deposited on top of PVF which showed no electrochemistry would demonstrate no holes exist in the film; however, no solvent could be found from which to perform

Fig. 5. SEM micrographs run at 25 kV, of copper on graphite. The Cu is approximately 0.2 μm thick. (a) Cu on rough graphite; (b) the same as (a) except Cu deposited through a PVF film; (c) Cu deposited through a 2 μm thick PVF film on well polished graphite. In both cases, PVF has been removed following Cu deposition. All figures are on the same scale; the white bar in each represents 10 μm. The right side of (a) and (b) are topographical micrographs; the remaining micrographs are compositional.

the deposition of the second layer that did not also solvate the PVF. Moreover, we found that when a PVF film electroprecipitated from dichloromethane did not appear to be uniformly deposited, soaking the film for a short time in a MeCN resulted in a film which, when dried, had a homogeneous appearance; similar effects with longer soaking, were observed for water. This observation and the above experimental results again indicate the polymer in an electrolytic solution is well represented as a liquidus phase at the electrode surface, even if the existence of pinholes is not totally precluded by these results.

SWELLING COEFFICIENT

All of the model parameters extracted from the experiments are ratios of the system parameters $K[D_m/D_s]^{1/2}$ and D_m/δ^2 for chronoamperometry and $P_m = KD_m/\delta$ for the RDE. The model parameters would be tractable if K, D_m, or δ were known independently. In an attempt to determine a relationship between the experimentally accessible dry thickness, d, and the experimentally inaccessible wetted thickness, δ, an experiment was performed where a film was deposited on a platinum flag, and cyclic voltammograms at 2 mV/s were obtained coulometrically to determine the moles of PVF/cm^2. The flag was then soaked in MeCN, equilibrating the polymer with the solvent and removing the excess electrolyte. (As electrolytic MeCN evaporated, it left a high and unknown concentration of $TBABF_4$ mixed with the polymer; the uncertainty in the electrolyte's weight and influence on the polymer's swelling necessitated the use of pure MeCN.) The solvent-sodden flag was removed from the MeCN and the weight change as the solvent evaporated was monitored as a function of time (Fig. 6). Initially, the solvent evaporated very rapidly and then reached a limiting weight. We used this weight of the polymer, flag, and solvent to determine the amount of solvent just needed to wet the film. At longer times (15 and 30 min), when the solvent has evaporated, a constant weight of the polymer and flag is found. The product of the solvent density and the difference of these two limiting weights corresponds to the volume of MeCN necessary to saturate the polymer, V_{MeCN}. If the PVF/MeCN interactions are taken to be ideal, two limiting cases can be used to estimate this volume. For an ideal solution, V_{MeCN} represents the volume of the swollen film, V_s. Alternatively, the polymer and solvent could be represented as two distinct phases, in which case the swollen volume is equal to the sum of V_{dry}, the solvent-free or dry volume of the polymer, and V_{MeCN}. V_{dry} is found from the charge passed in completely oxidizing or reducing of the film, Q_{film}, and the dry density of the polymer, ρ, where $V_{dry} = Q_{film} \times$ (molecular weight of the monomer)$/F\rho$. As the actual PVF/MeCN system probably lies somewhere between the solution and the two-phase representation, the experiment can be interpreted using $V_{MeCN} \leqslant V_s \leqslant V_{MeCN} + V_{dry}$. For a dry film on a rectangular substrate, $v_{dry} = l \times w \times d$, where l is the length and w is the width of the platinum flag, while d is the film thickness. If the wetted film is modelled as swelling uniformly in each direction not bound by the platinum substrate, $v_s = (l + 2\Delta l) \times (w + 2\Delta w) \times (d + \Delta d)$ where $\Delta l = \Delta w = \Delta d$. When $l \gg \Delta l$, $w \gg \Delta w$, and $l, w \gg d$, the

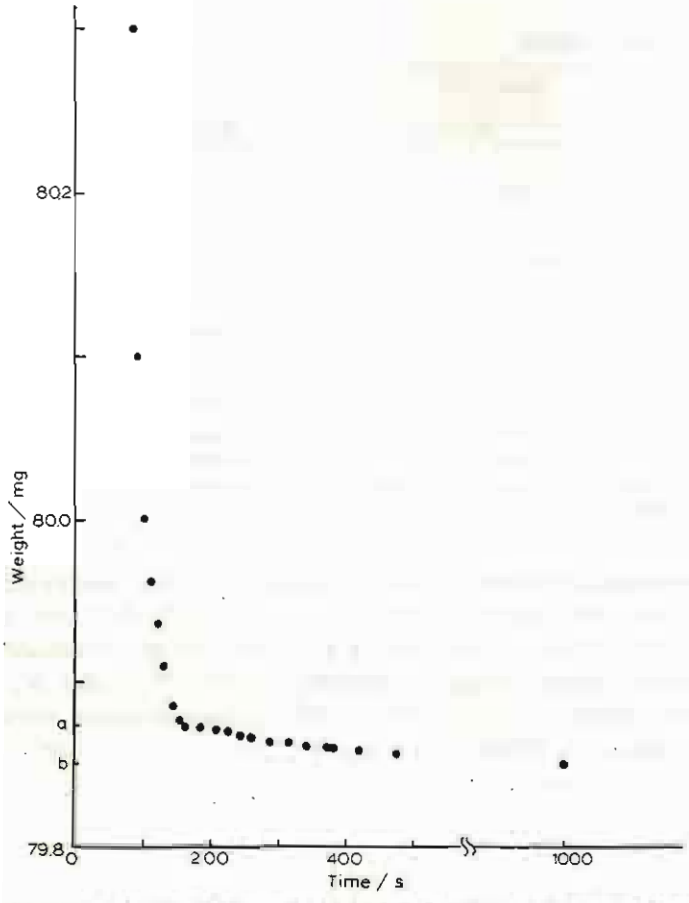

Fig. 6. Results of weighing experiments used to determined the thickness of the solvent-swollen film. The rate of solvent evaporation was monitored as a function of time. The break in the curve represents the weight of the polymer, flag and just enough solvent to wet the film, marked by (a). The weight at very long times is the weight of the polymer and flag alone, marked by (b). The weight of solvent corresponds to the degree of swelling in the film. This curve corresponds to Sample D in Table 3.

swollen volume is well represented as $v_s = lwd + lw\Delta d$, or $\Delta d = (v_s - v_{dry})/lw$. For a generalized substrate surface of area, A, where the dimensions of each surface coordinate are much greater than d, $\Delta d = (v_s - v_{dry})/A$. Therefore, the coefficient of swelling normal to substrate, ξ, where $\delta = \xi d$, is $1 + \Delta d/d$. Let $V_s = v_s$ and $V_{dry} = v_{dry}$; Table 3 presents the results. The dry density of PVF is taken as 1.25 g/cm^3. ξ_{min} and ξ_{max} arise from representing V_s as V_{MeCN} and $(V_{MeCN} + V_{dry})$, respectively. The results indicate $1.2 < \xi < 2.4$; so we have taken $\xi = 1.8$. Note that the swelling measurements were made with pure solvent; the presence of an electrolyte probably affects the degree of swelling.

From the swelling coefficient and the dry thickness, the value of D_m and K could

TABLE 2

Analysis of RDE data based on membrane model

		Steady state	
$10^5\, d_{dry}$/cm	c_x^*/m M	$Pm = KDm/\delta \times 10^3$	$KD_m \times 10^7$ [a]
MV			
4.42	1.92	2.65	2.12
BQ			
1.64	1.95	24.8	7.32
7.70	1.96	8.31	11.5
	3.89	5.76	7.98
	5.82	4.52	6.27
11.32	4.00	3.34	6.81
	6.02	2.65	5.40
	8.12	2.38	4.85

[a] Calculated with a swelling, ξ, of 1.8.

be extracted from the chronoamperometric results in Table 1. D_m was calculated from each value of D_m/δ^2; the averages are $D_m(MV^{+2}) = (3.9 \pm 1.6) \times 10^{-8}$ cm^2/s and $D_m(BQ) = (13.4 \pm 2.6) \times 10^{-8}$ cm^2/s. The value of K/γ and average membrane diffusion coefficient defined K, which is equal to 6.0 and 3.5 for MV^{+2} and BQ, respectively. The permeability values, listed in Table 2 for RDE measurements, were used to evaluate KD_m. The results in Table 2, are $KD_m(MV^{+2}) = 2.1 \times 10^{-7}$ cm^2/s and $KD_m(BQ) = (7.2 \pm 2.2) \times 10^{-7}$ cm^2/s.

TABLE 3

Determination of linear polymer swelling based on solvent evaporation rate as a function of time

	Sample A	Sample B	Sample C	Sample D
wt PVF/μg [a]	5.94	14.1	35.3	32.0
wt MeCN/μg	5.0	12.0	27.0	27.0
Area/cm^2	0.0728	0.0891	0.270	0.234
$10^6\, V_{dry}$/cm^3 [b]	4.75	11.3	28.2	25.6
$10^6\, V_{MeCN}$/cm^3 [c]	6.36	15.3	34.4	34.4
$10^5\, d_{dry}$/cm [d]	6.52	12.7	10.4	11.7
$10^5\, \Delta d_{min}$/cm [e]	2.21	4.49	2.30	4.04
$10^5\, \Delta d_{max}$/cm [f]	8.74	17.2	12.7	15.8
ξ_{min}	1.34	1.35	1.22	1.35
ξ_{max}	2.34	2.35	2.22	2.35

[a] Calculated from charge Q passed on a 2 mV/s cathodic sweep: $wt = Q/nF \times 213$ g mol^{-1}.
[b] Based on a dry density PVF = 1.25 g/cm^3.
[c] Density MeCN = 0.7857 g/cm^3.
[d] $d_{dry} = V_{dry}/\text{Area}$.
[e] $(V_{MeCN} - V_{dry})/\text{Area} = \Delta d_{min}$.
[f] $V_{MeCN}/\text{Area} = \Delta d_{max}$.

TABLE 4

Summary of experimentally determined D_m and K for MV^{+2} and BQ

	MV^{+2}	BQ
Chronoamperometry		
$D_m/cm^2\ s^{-1}$	4×10^{-8}	1×10^{-7}
K	6	4
$KD_m/cm^2\ s^{-1}$	2.4×10^{-7}	4.0×10^{-7}
RDE		
$KD_m/cm^2\ s^{-1}$	2.1×10^{-7}	7.2×10^{-7}

The experimental results are summarized in Table 4. The product of the chronoamperometrically determined D_m and K shows reasonably good agreement with the RDE results, considering the precision of the data and needed approximations. The values of D_m are also consistent with the results of Schroeder and Kaufman [11], who monitored the diffusion of an organic dye, Sudan III, out of a PVF film spectroscopically and concluded that $D_m > 10^{-9}$ cm^2/s. The chronoamperometric results show the diffusion coefficient in solution is approximately 200 times larger than in the membrane for MV^{+2} and BQ. If the polymer in an electrolytic solution is envisioned as a viscous liquid, by application of Walden's rule [6b] the surface confined PVF/MeCN system has a viscosity similar to cyclohexanol ($\sim$ 0.6 poise). An alternative method [12] has been proposed for determining D_m and K chronoamperometrically, and used with Nafion films. In this method, the polymer initially contains none of the redox couple present in solution and the rate at which it enters the film is determined. This method could be used to determine D_m and K. However, because D_m is approximately 10^{-8} cm^2/s and δ about 1 μm, for PVF, the redox couple diffuses into the polymer within 250 ms, a period too brief to be useful under normal chronoamperometric conditions.

ACKNOWLEDGEMENTS

Dr. Michael Schmerling's assistance with the electron microscopy is appreciated. The support of this research by the National Science Foundation (CHE 7903729) is gratefully acknowledged.

REFERENCES

1 T. Gueshi, K. Tokuda and H. Matsuda, J. Electroanal. Chem., (a) 89 (1978) 247; (b) 101 (1979) 29.
2 P.J. Peerce and A.J. Bard, J. Electroanal. Chem., (a) 112 (1980) 97; (b) 114 (1980) 89.
3 D.A. Gough and J.K. Leypoldt, (a) Anal. Chem., 51 (1979) 439; (b) A.I. Ch. E. J., 26 (1980) 1013; (c) Anal. Chem., 52 (1980) 1126; (d) J. Electrochem. Soc., 127 (1980) 1278.
4 T.W. Smith, J.E. Kuder and D. Wychik, J. Polym. Sci. Polym. Chem. Ed., 14 (1976) 2433.
5 A. Merz and A.J. Bard, J. Am. Chem. Soc., 100 (1978) 3222.
6 A.J. Bard and L.R. Faulkner, Electrochemical Methods, Wiley, New York, (1980), (a) p. 143; (b) p. 154.

7 R. Szentrimay, P. Yeh and T. Kuwana, Paper presented at 172nd National ACS meeting, San Francisco, August, 1976.
8 M. Umana, P. Denisevich, D.R. Rollison, S. Nakahama and R.W. Murray, Anal. Chem., 53 (1981) 1170.
9 T. Ikeda, R. Schmehl, P. Denisevich, K. Willman and R.W. Murray, J. Am. Chem. Soc., 104 (1982) 2684.
10 (a) F. Scheller, S. Müller, R. Landsberg and H.J. Spitzer, J. Electroanal. Chem., 19 (1968) 187; (b) F. Scheller, R. Landsberg and S. Müller, J. Electroanal. Chem., 20 (1969) 375; (c) R. Landsberg and R. Thiele, Electrochim. Acta, 11 (1966) 1243.
11 A.H. Schroeder and F.B. Kaufman, J. Electroanal. Chem., 113 (1980) 209.
12 H.S. White, J. Leddy and A.J. Bard, J. Am. Chem. Soc., 104 (1982) 4811.